Journal of Physics: Conference Series **568** (2014) 032020 doi:10.1088/1742-6596/568/3/032020

Application of low frequency SQUID NMR to the ultra-low temperature study of atomically layered ^{3}He films adsorbed on graphite

F. Arnold, B. Yager, J. Nyéki, A. J. Casey, A. Shibahara, B. P. Cowan and J. Saunders

Royal Holloway, University of London, TW20 0EX Egham, United Kingdom

E-mail: b.yager@rhul.ac.uk, j.saunders@rhul.ac.uk

Abstract. Low frequency pulsed NMR is a powerful technique for the investigation of the nuclear susceptibility and spin-dynamics of strongly correlated systems down to ultra-low temperatures. We describe a versatile broadband pulsed NMR spectrometer using a two-stage Superconducting Quantum Interference Device (SQUID). This instrument has enabled the investigation of the spin-dynamics of ^{3}He films adsorbed on exfoliated graphite into the microkelvin temperature range. In prior work we reported a SQUID NMR study of two-dimensional ferromagnetism on a triangular lattice, where ^{3}He films adsorbed on graphite provide an ideal model system. Here we describe the detection of the much weaker signals from strongly correlated fluid films in the second layer of ^{3}He on graphite, using a spectrometer with improved sensitivity. We have measured the low frequency spin-spin relaxation and spin-lattice relaxation of two-dimensional ^{3}He into the microkelvin range. These show an unusual time and frequency dependence. We also describe the use of the ^{13}C-signal from the exfoliated graphite for thermometry, and the unusual properties of the spin-lattice relaxation of that system.

1. Introduction

Helium isotopes adsorbed onto the atomically flat basal planes of exfoliated graphite provide model systems for the investigation of quantum matter in two dimensions. For an overview and a review of earlier work see [1]. These atomically layered films provide a quantum simulator to further the understanding of key contemporary problems in condensed matter physics including: frustrated magnetism [2, 3]; heavy-fermion quantum criticality [4]; the Mott-Hubbard transition [5]. NMR provides a powerful tool to study ^{3}He films, but until now the focus of measurements at ultra-low temperatures has been on studies of a static property, the ^{3}He nuclear magnetization, complementing measurements of heat capacity. While NMR studies of spin dynamics played a central role in the pioneering studies of ^{3}He submonolayer films on graphite [6, 7], their use in measurements at ultra-low temperatures have so far been limited. In this article we briefly survey our recent work to apply SQUIDs to the detection of NMR signals at relatively low frequencies. The gains are: improved precision in the measurement of magnetization; the ability to conveniently measure as a function of magnetic field; the ability to study spin-dynamics into the microkelvin range.

2. The Spectrometer

Our pulsed NMR spectrometer includes a helium adsorption cell and home-made NMR magnet assembly mounted at the demagnetization stage and mixing chamber of a dilution refrigerator respectively.

The adsorption cell contains a stack of 64 exfoliated graphite sheets (Grafoil [8]), enclosed in a Stycast-1266 body [9]. The cell is oriented such that the Grafoil sheets are normal to the static NMR field B_0. In Grafoil, graphite platelets show a preferential alignment of their c-axis normal to the foil surface. The mosaic spread of these platelets was found to be $\pm 19°$ [2] for a sample from the same batch. In the cell, each Grafoil sheet is individually heatsunk to the experimental stage through a diffusion bonded silver foil which is connected to the central thermal anchor of the cell (see Fig. 1). Helium can be admitted to the cell via a narrow fill line that extends up to a room temperature gas handling system. The total surface area of the graphite substrate is $12\,\mathrm{m}^2$ as determined from point-B of a ^{4}He adsorption isotherm at 4.2 K [10].

The low field NMR magnet and coil assembly is contained within a 31 mm diameter, 105 mm long superconducting niobium shield and is of a similar design to those described previously [11]. The NMR magnet is a 4 layer solenoid wound using 106 µm CuNi clad NbTi wire. The transmitter coil is wound around a 25 mm diameter former using similar wire following the optimum saddle coil geometry described by Hoult and Richards [12] and has a field current ratio of $0.275\,\mathrm{mT\,A^{-1}}$. An overlapping superconducting Hechtfischer [13] shield between the NMR magnet former and transmitter coil screens eddy-current transients in the copper induced by transmitter pulses.

The receiver coil is wound directly onto the epoxy sample cell using NbTi wire and has a 10 mm square cross-section. The NMR cell is mechanically and thermally decoupled from the magnet assembly in order to reduce magneto-acoustic resonances and heat leaks into the nuclear demagnetization stage. Orthogonality of the transmitter and receiver coils is optimized whilst assembling the setup by cross-coupling measurements.

NMR signals are coupled into the SQUID amplifier by a superconducting flux transformer

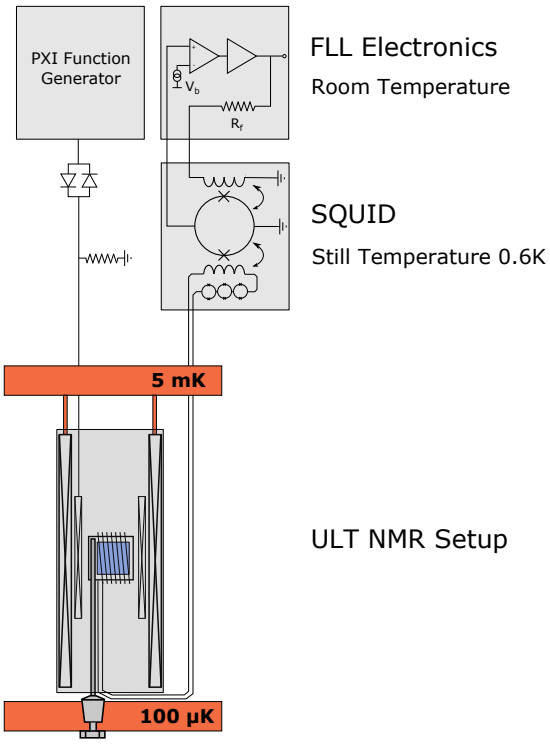

Figure 1. Schematics of the ultra-low temperature SQUID NMR setup. The NMR cell is mounted on the 100 µK-plate of a nuclear demagnetization stage whereas the magnet assembly is supported by the mixing chamber. NMR signals are coupled into a two-stage DC-SQUID, which is controlled by a room-temperature FLL electronics. Tipping pulses are generated with a PXI arbitrary waveform generator.

consisting the receiver coil and the integrated SQUID input coil, which are connected by a superconducting twisted pair shielded by a niobium capillary. Both coils have matching inductances of $L_i = 1.8\,\mu\text{H}$ to maximize the flux transfer ratio. This set-up provides a broadband detection scheme allowing measurements at different B_0, and hence NMR frequencies.

We use a two stage DC-SQUID with integrated current limiter developed by PTB [14]. When operated in flux-locked loop mode (FLL) [15] it serves as a low noise, high bandwidth, high gain flux-to-voltage converter. Control and feedback for the the SQUID is provided by room-temperature Magnicon XXF-1 FLL electronics with 6 MHz bandwidth [16]. The coupled energy sensitivity of our spectrometer is $\varepsilon_c = L_i S_\phi / 2M_i^2 = 9.1\,h$, where M_i is the mutual inductance between the input coil and SQUID and S_ϕ the flux noise per unit bandwidth, with the SQUID cooled to 700 mK.

NMR pulse sequences and signal acquisition are controlled by a National Instruments PXI system [17]. Tipping pulses are produced by a PXI-5412 arbitrary waveform generator and the resultant NMR signals captured by a PXI-5922 digitizer with 20-bit resolution at 5MS/s [17]. A 4 kHz high-pass filter is used to attenuate low frequency eddy-current transients. The captured signals are background-subtracted with an off-resonance and zero-field transient to eliminate magneto-acoustics around the Larmor frequency and low-frequency transients respectively. The signals are analyzed in the frequency domain by applying a conventional FFT. However the exceptionally high signal-to-noise ratio also permits study directly in the time domain by using lock-in demodulation; this allows us to see the precise shape of the recorded free induction decays (FIDs).

3. 2D ^{3}He Adsorbed on Graphite at Ultra-Low Temperatures

This section describes pulsed NMR measurements on a monolayer ^{3}He film sample with areal density $5.5\,\text{nm}^{-2}$ adsorbed onto graphite preplated by a monolayer of ^{4}He, to highlight the versatility of our broadband spectrometer. We show magnetization, spin-spin and spin-lattice relaxation time measurements of this strongly correlated 2D Fermi fluid.

3.1. Nuclear Susceptibility

The nuclear susceptibility of the sample was measured at 100 kHz and temperatures from 240 µK to 10 mK during the natural warmup of the demagnetization stage and from 6 mK to 300 mK using thermally stabilized data points. The magnetization was determined from a stretched exponential fit to the envelope function of the FID in the time-domain. Figure 2 shows the temperature dependence of the total magnetization. The data is fitted by a Curie-Weiss, plus a Dyugaev Fermi fluid magnetization [18] of the form:

$$MT = \frac{N_1 C}{1 + \Theta/T} + \frac{N_2 C}{\sqrt{1 + (T_F^{**}/T)^2}}, \tag{1}$$

where C is the Curie constant per spin, Θ the Curie temperature and T_F^{**} the renormalized Fermi temperature. The first term phenomenologically describes an upturn above the Pauli susceptibility at lowest temperatures. We find an effective Fermi temperature, $T_F^{**} = 131\,\text{mK}$, consistent with previous measurements [19]. We used the Landau Fermi liquid susceptibility enhancement $\chi/\chi_0 = (m^*/m)(1 + F_0^a)^{-1}$, together with the fact that the spin-antisymmetric Landau parameter $(1 + F_0^a)^{-1} = (1 + \sqrt{1 - m/m^*})^2$ depends weakly on effective mass [5, 18, 19], to obtain an effective mass of $5.8 \pm 0.2\,m_0$. This effective mass is consistent with data obtained by Greywall [20] when density corrections due to first layer compression [21] are taken into account, and also with results of Lusher [22, 23] and Morhard [24].

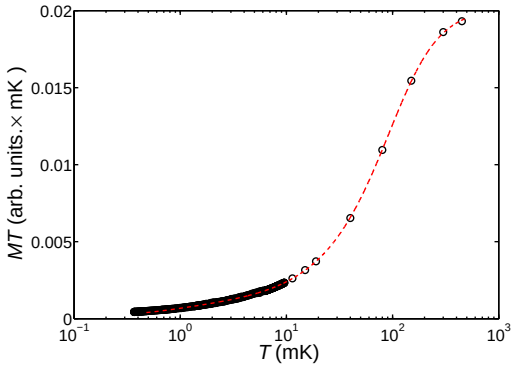

Figure 2. Sample magnetization measured over 3 orders of magnitude in temperature, obtained using small angle tipping pulses. The dashed line shows a fit to Eq. 1.

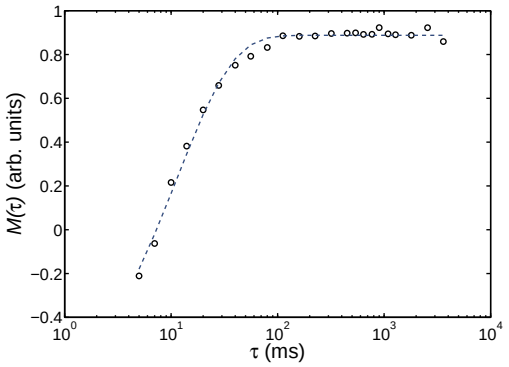

Figure 3. A 750 µK measurement of T_1 at 100 kHz made using an inversion-recovery pulse sequence. The vertical scaling is relative to the magnetization obtained using the same readout pulse, without the preparation pulse, before the measurement. The data (open circles) is fitted by an exponential decay (dashed blue line)

3.2. Spin-Spin relaxation

The transverse relaxation times T_2^* were extracted from fits to the Fourier transformed FIDs. Since T_2^* includes contributions from both intrinsic spin-spin interactions and from inhomogeneities in the static magnetic field, measurements of the intrinsic T_2 are desirable. T_2 was measured using the usual $90° - \tau - 180° - \tau$−spin-echo pulse sequence, requiring additional hardware. A Stanford DG535 delay generator provided a precise trigger source for two Agilent 33220A arbitrary waveform generators and for the PXI digitizer. An example of the quality of data obtained for a spin-echo measurement is shown in Fig. 4.

Fig. 5 shows the spin-echo heights as a function of delay, τ, for frequencies between 100 and 300 kHz. Here the decay of the magnetization was well described by a superposition of two exponential functions, as previously found for similar systems [25, 26]. We observe that the shorter component $T_{2S} = 14.8$ ms is frequency independent whilst the relaxation rate of the longer component increased non-linearly with increasing frequency (see inset Fig. 5) in contrast to previous measurements at higher frequencies [26]. Here the low frequency T_2 is governed by the intrinsic dipole-dipole interaction [27]. The magnetization of the shorter component was an order of magnitude larger than that of the longer component.

3.3. Spin-Lattice Relaxation

Measurements of the spin-lattice relaxation time of adsorbed ^{3}He have previously been used to, for example, measure exchange [28] and dimensionality at $T > 1$ K [29]. Fig. 3 shows a preliminary measurement of T_1, using a $180° - \tau -$ readout sequence, where the sample was at 750 µK before the measurement. Here the vertical scale is the magnetization normalized to its equilibrium value before each data point was taken, sampled with a 0.6° pulse. The 11% reduction of magnetization at long τ is due to an overheating of the sample during the measurement and corresponds to a temperature increase of 80 µK using the magnetization data in Fig. 2.

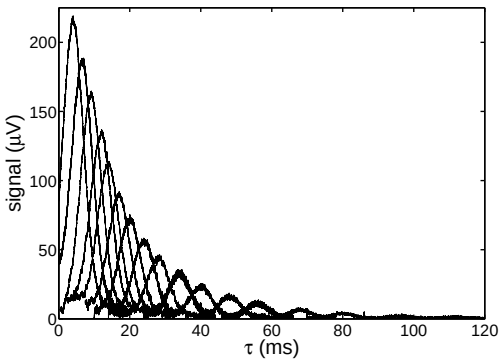

Figure 4. Spin-echoes obtained from a $90° - \tau - 180° - \tau$−spin-echo pulse sequence at 20 mK and 100 kHz. A digital lock-in technique was used to demodulate the data before fitting. The peak height of the echoes obtained from the fits, plotted in Fig. 5, was used to determine T_2.

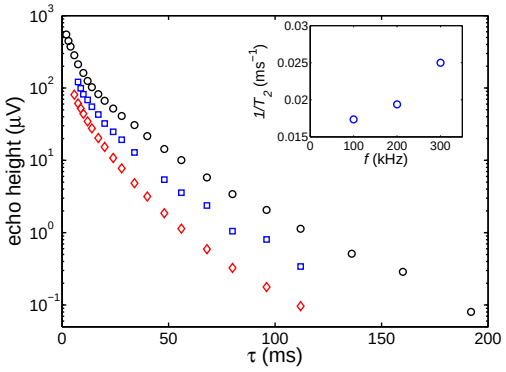

Figure 5. Results of spin-echo measurements at 20 mK. The plotted data is of the peak height of the spin echoes analysed in the time-domain using a digital lock-in technique. (○) 100 kHz, (□) 200 kHz, (◇) 300 kHz. $1/T_2$ for the long components are plotted in the inset. The gain of the amplifier was changed for different frequencies to avoid saturation.

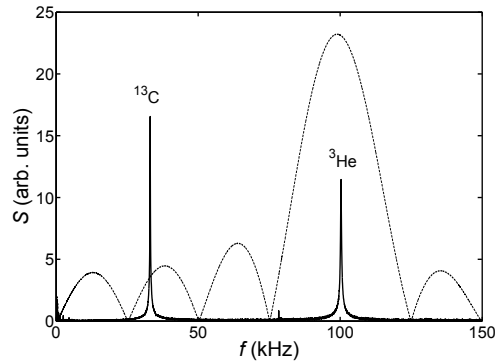

Figure 6. Frequency spectrum of a FID at 370 μK (solid line) showing the on-resonance ^{3}He signal of the 5.5 nm^{-2} sample and the ^{13}C signal of the substrate excited by the power spectrum wing of the excitation pulse (dashed line).

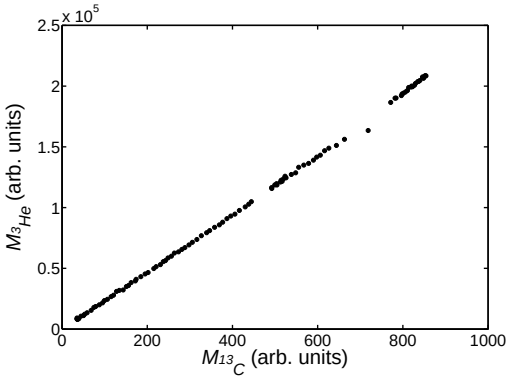

Figure 7. Carbon vs helium magnetizations of a pure ^{3}He sample, where both helium and carbon nuclei are paramagnetic. The ^{13}C is used as the main experimental thermometer below 1 mK. Data in this figure goes down to 250 μK.

4. ^{13}C NMR Thermometry

In our setup we used the spin-½ ^{13}C nuclei present in the Grafoil substrate, at a natural abundance of 1.1 %, as a thermometer below 1 mK. This enabled us to measure directly the temperature of the substrate, which should have the smallest possible temperature gradient to the helium sample. Within graphite ^{13}C forms a dilute nuclear paramagnet with weak dipole-dipole interactions and hence a narrow NMR line width ($T_2^* = 2.4$ ms).

An advantage of the broadband spectrometer is that it allows us to observe FIDs from ^{3}He

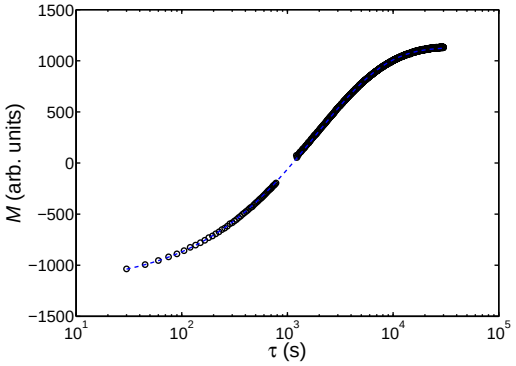

Figure 8. T_1 relaxation of ^{13}C measured at 500 µK following a 180° excitation pulse. The recovering magnetization was probed by small-angle tipping pulses. The data (open circles) is fitted to a stretched exponential relaxation with exponent $n = 0.65$ and $T_1 = 1860$ s (dashed blue line).

and ^{13}C simultaneously. ^{13}C has a gyromagnetic ratio of $\gamma_{^{13}C} = 10.8\,\mathrm{MHz\,T^{-1}}$, compared to $\gamma_{^3He} = 32.4\,\mathrm{MHz\,T^{-1}}$. Fig. 6 shows the magnitude of a FFT of a 40 µs transmitter pulse at 100 kHz, demonstrating that there is significant spectral power over a broad frequency range. Fig. 6 also shows a FFT of the NMR response to this pulse where $B_0 = 3.08$ mT, so that the ^{3}He is on resonance and the ^{13}C resonance is close to the second side maximum of the pulse power spectrum.

The magnetization of the ^{13}C is obtained from a Lorentzian fit to the complex FFT of the FID. This is calibrated against the ^{3}He melting curve thermometer, MCT, over the temperature range 5.5 mK to 20 mK using thermally stabilised data points. The MCT is self-calibrated against the superfluid A-transition.

The thermal coupling of the ^{13}C and the adsorbed helium sample is demonstrated in Fig. 7 where the magnetization of the ^{13}C is compared to that of a pure bilayer ^{3}He film of areal density $13.0\,\mathrm{nm^{-2}}$, for which the first layer paramagnetism strongly dominates at low temperatures. The linearity shows that both spin species were in thermal equilibrium over the entire temperature range.

Since the pulse repetition rate of NMR thermometers at ultra-low temperatures is limited by their T_1 relaxation time, we investigated the longitudinal recovery of ^{13}C down to the lowest temperatures. The T_1 recovery of the ^{13}C, shown in Fig. 8, was measured using small angle tipping [30], where the equilibrium magnetization was initially prepared by a 180° pulse and the recovery is subsequently probed by repeated 2° tipping pulses. The recovery is fitted by a stretched exponential according to:

$$M\left[\tau\right] = M\left[\infty\right] - \left(M\left[\infty\right] - M\left[0\right]\right) e^{-(\tau/T_1)^{\alpha}}, \tag{2}$$

where τ is the time between the preparation pulse and readout pulse and α is a fitting parameter. Non-exponential relaxation is commonly observed where a continuous range of relaxation times exist, see for example [31]. However, we find that the exponent $\alpha = 0.65$ is close to ⅔, which is the expected value for a 2D rigid lattice of spins [30], suggesting that relaxation may be due to a low dimensional effect.

5. Summary

We have installed a versatile broadband NMR spectrometer to measure samples thermalized to a nuclear demagnetization stage. The broadband nature of the spectrometer allows both frequency and temperature as tuning parameters. The nuclear magnetization of ^{13}C within the graphite substrate has been used as a thermometer below 1 mK and is shown to be well thermalized to the ^{3}He film sample. We have demonstrated the feasibility of measuring T_1, T_2,

T_2^* and the nuclear magnetism of ^{3}He films on graphite with high precision. This is currently being applied to the study of quantum criticality of the Mott-Hubbard transition and to identify a possible quantum-spin liquid phase. This work has been financially supported by EPSRC grant EP/H048375/1.

References

[1] Godfrin H and Lauter H J 1995 *Prog. Low Temp. Phys.* **14** 213 – 320
[2] Casey A J, Neumann M, Cowan B, Saunders J and Shannon N 2013 *Phys. Rev. Lett.* **111** 125302
[3] Fukuyama H 2008 *J. Phys. Soc. Jpn* **77** 111013
[4] Neumann M, Nyéki J, Cowan B and Saunders J 2007 *Science* **317** 1356
[5] Casey A J, Patel H, Nyéki J, Cowan B P and Saunders J 2003 *Phys. Rev. Lett.* **90** 115301
[6] Cowan B P 1980 *J. Phys. C: Solid State Phys.* **13** 4575
[7] Owers-Bradley J R, Thomson A L and Richards M G 1978 *J. Phys. Colloques* **39**(C6) 298
[8] Grafoil is a product of GrafTech International Advanced Electronics Technology, 11709 Madison Ave. Lakewood, OH 44107, United States, formerly UCAR - http://www.graftech.com
[9] Stycast is a product of the Henkel Corporation, One Henkel Way, Rocky Hill, CT 06067, USA
[10] Bretz M, Dash J G, Hickernell D C and Vilches O E 1973 *Phys. Rev.* B **8** 1589
[11] Lusher C, Li J, Digby M, Reed R, Cowan B, Saunders J, Drung D and Schurig T 1999 *Applied Superconductivity* **6** 591
[12] Hoult D I and Richards R E 1976 *J. Magn. Reson.* **24** 71
[13] Hechtfischer D 1987 *Cryogenics* **27**(9) 503
[14] Drung D, Assmann C, Beyer J, Kirste A, Peters M, Ruede F and Schurig T 2007 *IEEE Trans. Appl. Supercond.* **17** 699–704
[15] Drung D 1996 *Advanced Squid Read-Out Electronics* vol 329 (Springer Netherlands)
[16] Drung D, Hinnrichs C and Barthelmess H J 2006 *Supercond. Sci. Technol.* **19** S235
[17] National Instruments Corporation 11500 N Mopac Expwy Austin TX 78759-3504
[18] Dyugaev A M 1990 *Sov. Sci. Rev. A Phys.* **1**
[19] Bäuerle C, Bunkov Y M, Chen A S, Fisher S N and Godfrin H 1998 *J. Low Temp. Phys* **110** 333
[20] Greywall D S 1990 *Phys. Rev.* B **41**(4) 1842–1862
[21] Roger M, Bäuerle C, Godfrin H, Pricoupenko L and Treiner J 1998 *J. Low. Temp. Phys* **112**(5) 451
[22] Lusher C P, Saunders J and Cowan B P 1991 *Europhys. Lett.* **14** 809
[23] Lusher C P, Cowan B P and Saunders J 1991 *Phys. Rev. Lett* **67** 2497
[24] Morhard K D, Bäuerle C, Bossy J, Bunkov Y, Fisher S N and Godfrin H 1996 *Phys. Rev.* B **53** 2658
[25] Neumann M, Casey A J, Levitin L, Cowan B and Saunders J 2010 *J. Low. Temp. Phys* **158**
[26] Takayoshi S, Obata K, Sato D, Matsui T and Fukuyama H 2009 *J. Phys.: Conf. Series* **150** 032104
[27] Cowan B, El-Nasr L A, Fardis M and Richards M 1987 *Jpn. J. Appl. Phys.* **26** 309–310
[28] Cowan B, El-Nasr L A, Fardis M and Hussain A 1987 *Phys. Rev. Lett.* **58** 2308
[29] Yager B, Nyéki J, Casey A, Cowan B P, Lusher C P and Saunders J 2013 *Phys. Rev. Lett* **111**(21) 215303
[30] Cowan B P 1997 *Nuclear Magnetic Resonance and Relaxation* (Cambridge University Press)
[31] Narayanan A, Hartman J S and Bain A D 1995 *J. of Magn. Reson. Series* A **112** 58